Synthesis and performance of pomegranate peel-supported zero-valent iron nanoparticles for adsorption of malachite green

Figen Gündüz, Bahar Bayrak*

Chemical Engineering Department, Engineering Faculty, Atatürk University, 25240 Erzurum, Turkey, Tel. +90442 2314518; email: batabek@atauni.edu.tr (B. Bayrak), Tel. +90534 2323294; email: figengunduz08@gmail.com (F. Gündüz)

abstract

Nanoscale zero-valent iron (NZVI) supported by carbonized pomegranate peel (CPP) was synthesized by liquid-phase chemical reduction and characterization of the composites was carried out with Fourier transform infrared spectroscopy, scanning electron microscopy, X-ray diffraction, pH_{zpc} (zero point of charge) and Brunauer–Emmett–Teller. NZVI/CPP composites were tested as adsorbents in the disposal of malachite green (MG) with certain parameters. The maximum adsorption value of MG was obtained as 99.7% for the adsorbent dose of 0.15 g in 30 min of equilibration time. The most suitable isotherm was obtained as the Langmuir isotherm (R^2 = 0.98) with the analysis of equilibrium data, and the maximum adsorption capacity (q_m) was found as 32.47 mg/g. The pseudo-second-order kinetic model ($R^2 \geq 0.994$) was found to be the best fit to the experimental data in comparison with the other models. The experimental results obtained at different temperatures were analyzed and adsorption was determined to occur endothermically and spontaneously due to the $\Delta H°$ value of 110.27 kJ/mol and $\Delta G° \leq -0.89$ kJ/mol, respectively. The positive values of $\Delta S°$ indicated that the irregularity in the interface between the NZVI/CPP adsorbent and the MG solution increased. NZVI/CPP may be used instead of active carbon for dye removal in industrial wastes due to its low cost and good performance.

Keywords: Malachite green; Pomegranate peel; Nano zero-valent iron; Isotherm; Kinetics; Thermodynamics

1. Introduction

Developing technology causes an increase in consumption of dyes in industrial processes. Synthetic dyes are used in many industries such as paint, plastics, paper, cosmetics, printing, electroplating, leather, wool, textile and pharmaceutical industries [1–3] and wastewater contaminated with dye is discharged into the seas, lakes, rivers and soil because of difficulties in degradation. Malachite green (MG) is a basic and cationic dye which is used for coloring cotton, silk, paper and leather and also as a pesticide [1]. MG is known to be carcinogenic, toxic and mutagenic for biota and humans [4]. Thus, discharge of wastewater including MG without purification causes great environmental problems.

There are many techniques used to purify wastewater [3,5,6]. Chemical techniques such as coagulation and flocculation are inadequate for dyes with high solubility. Biological techniques are insufficient in continuous treatment processes. Physical techniques such as ozonization, electrochemical degradation, adsorption and filtration are quite effective in removal of dyes from wastewater. Most of these methods are quite expensive and non-selective, and they cause formation of by-products or sludge. However, adsorption is the best technique for wastewater disposal in comparison with other methods because of its plainness of system, high performance and low cost [3,5].

In adsorption processes, activated carbon with high adsorption capacity has been the most frequently used adsorbent, but it has a high cost. Therefore, researchers aim

* Corresponding author.

to find new natural materials instead of activated carbon. Natural materials used as adsorbents are present in very large quantities in the nature and are preferred due to their non-toxicity, low cost and biodegradability. Organic waste materials such as hazelnut husk, pomegranate peel, oat hull, soy bean, forest waste, almond shell and minerals such as clay, pumice, alumina and zeolite were evaluated for wastewater treatment [1–3,6–13].

Pomegranate is used as both fresh fruit and raw material in manufacturing juice, jams and wine. Pomegranate peel is a waste organic material remaining from this consumption and it is costless [14,15]. Therefore, it has begun to be preferred for use as an adsorbent [9,14–16]. However, adsorption capacities of such waste materials are generally low. Different chemical treatments are applied on adsorbents to increase their adsorption capacities [14,17,18].

Researchers work on various materials to improve catalytic activity. Metal nanoparticles with monometallic (i.e., Pd, Pt), bimetallic (i.e., Au/Pt) and trimetallic (i.e., Cu/Pd/Fe) combinations are among these materials [19]. Metal and metal oxide nanoparticles are used in many areas such as heterogeneous catalysts, medicinal applications, environmental remediation and disinfection. Katwal et al. [20] used copper oxide nanoparticles, which are metal oxides, as a photocatalyst for organic dye degradation. Nanoscale zero-valent iron (NZVI), a monometallic material, has a large surface area and high activity on the surface. It has recently been used increasingly in wastewater treatment [21–23]. However, it may be easily agglomerated because its particles are very small and they react with water and other components. It is also difficult to separate nanoparticles from wastewater. Therefore, it needs to be modified with a supporting material. This way, the aforementioned problems can be solved considerably. Materials such as zeolite, chitosan, cellulose, oyster, rubber seed, active carbon and clay were used as supporting materials [24–30]. At the same time, effective waste removal was carried out with nanomaterials that were formed by binding ZrO_2/Fe_3O_4 or Fe_3O_4 onto support materials such as chitosan and trisodium citrate [31,32]. The resulting inorganic/organic nanocomposites may be used both as an adsorbent and as a photocatalyst in purification of wastewater. These materials are preferred because they are multifunctional and selective [33,34]. However, the use of biomass waste as a support material is very limited [29,35].

For the objective of this study, zero-valent iron nanoparticles supported with carbonized pomegranate peel (CPP) was synthesized for use as an adsorbent and the study investigated the effects of parameters such as temperature, contact time, pH, initial MG concentration and adsorbent dose in removal of MG by this adsorbent. Both kinetic and isotherm models and thermodynamics parameters for adsorption process were obtained from the experimental data.

2. Materials and methods

2.1. Chemical reagents

MG with 99.0% purity, supplied by Merck (Darmstadt, Germany), was used as an adsorbate. A 1,000 mg/L stock solution was produced by dissolving MG in deionized water. MG has the chemical formula of $C_{23}H_{26}N_2Cl$ with a molecular weight of 364.92 g/mol and λ_{max} of 617 nm. The pH of MG solutions was adjusted with analytical grade HCl and NaOH solutions. Iron(II) chloride tetrahydrate ($FeCl_2 \cdot 4H_2O$), which is used for production of NZVI/CPP, was obtained from Acros Organics (Belgium). $NaBH_4$ and polyethylene glycol (PEG-400) were obtained from Merck. Ethanol (99.8%) was provided from Sigma Aldrich (St. Louis, MO, USA).

2.2. NZVI/CPP composites preparation

Pomegranates were obtained from the local market. The peels were then separated from other parts such as seeds, membranes and fruit. They were divided into small parts, washed with distilled water several times to discard impurities and dried at 100°C for 24 h to remove the moisture content. Later, they were crushed by a grinder, placed in a tightly closed stainless steel vessel, carbonized in a muffle furnace at 800°C temperature and with N_2 flow rate of 100 mL/min for 90 min, and finally sieved into particle sizes of 90–180 μm. The prepared pomegranate peels (CPP) were stored for use in the next step.

Synthesis of the NZVI/CPP composite can be carried out by liquid-phase reduction. 1.83 g of $FeCl_2 \cdot 4H_2O$ was dissolved in 50 mL of 30% (v/v) ethanol solution, 0.5 g PEG was added as the surfactant to this solution, and they were placed into a three-necked flask containing 1.0 g of CPP. The mixture was stirred with nitrogen gas for 1 h and then 100 mL of 1.61 mol/L $NaBH_4$ which was prepared with ethanol was added into the mixed solution at a rate of 30 drop/min. After all the $NaBH_4$ was added, the mixing process was continued for another 30 min under a nitrogen atmosphere. The mixture containing black particles was filtered and then the black particles were washed with both 30% (v/v) ethanol solution and distilled water. Finally, they were dried at 30°C for 5 h [35].

2.3. Adsorption experiments with the NZVI/CPP adsorbent

Adsorption of MG onto the synthesized NZVI/CPP was studied for parameters such as pH of the solution, contact time, initial MG concentration, NZVI/CPP dose and temperature. 50 mL solutions were taken into a 300 mL Erlenmeyer flask and the effect of each parameter was investigated by keeping the other parameters constant. The constant parameters were taken as temperature 40°C, pH 5, initial concentration 40 mg/L, adsorbent dose 0.1 g and contact time 30 min. Then, this solution was shaken in a water bath at a constant temperature and 250 rpm stirring speed (Edmund bühler TH15/KS15) by adding the adsorbent (Fig. 1). The samples were withdrawn at regular intervals from 1 to 150 min, the adsorbent was taken from the solution by centrifuging and the MG concentration remaining in the solution was analyzed by a UV–visible spectrophotometer (Thermo Elektron Corporation Evolution 500) at a maximum wavelength of MG (λ_{max} = 617 nm).

Adsorption capacity, q_e of NZVI/CPP and the removal % of MG were found with Eqs. (1) and (2), respectively.

$$q_e = \frac{C_o - C_e}{m} \cdot V \tag{1}$$
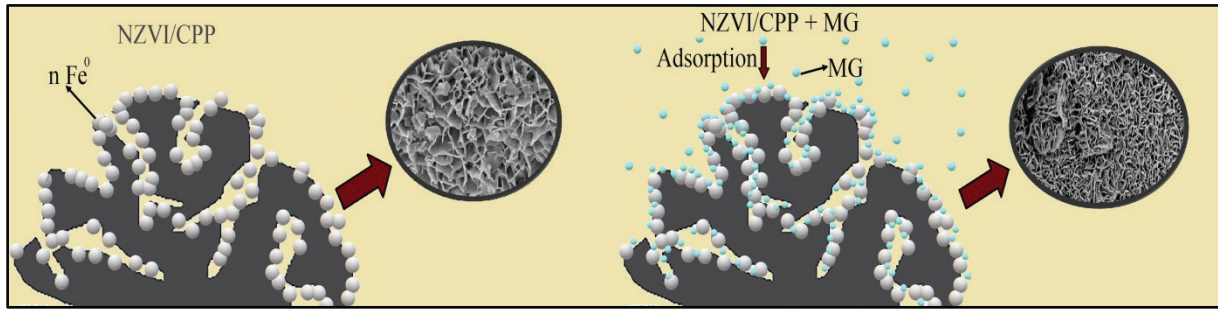
Fig. 1. A diagram showing the relationship between MG adsorbate and NZVI/CPP adsorbent.

$$\%\text{Removal} = \frac{C_o - C_e}{m} \cdot 100 \qquad (2)$$

where q_e is the amount of adsorbed MG per gram of NZVI/CPP (mg/g); C_o is the initial solution concentration (mg/L); C_e is the concentration of MG remaining in the solution at a certain time (mg/L); V is the initial solution volume (L) and m is the amount of NZVI/CPP (g).

3. Results and discussion

3.1. Characterization of CPP and NZVI/CPP

The surface morphologies of CPP in Fig. 2(a), the NZVI/CPP in Fig. 2(b) and the NZVI/CPP after adsorption in Fig. 2(c) were analyzed with a scanning electron microscope (SEM, Zeiss/Sigma 300). The samples were first coated in gold film to ensure conductivity, then placed in the sample unit and examined under high vacuum. The accelerating voltage was 2 kV and magnifications of images were changed between 29 and 204K. It was seen that holes formed on the CPP surface due to carbonization in Fig. 2(a). It was compounded with NZVI to further increase the surface area of the CPP. It could be seen that the surface of the adsorbent had a newly formed highly porous structure in Fig. 2(b) and it appeared that these pores were filled with some MG after adsorption in Fig. 2(c).

The surface functional groups and surface chemistry of the adsorbents were displayed by Fourier transform infrared spectroscopy (FTIR; Bruker VERTEX 70v). First, the dry sample was pelleted for analysis by mixing with KBr and then spectrums were obtained with a resolution of 4 cm⁻¹ and in the range of the wavelengths of 400–4,000 cm⁻¹ for CPP, NZVI/CPP and post-adsorption NZVI/CPP. The FTIR spectrums are shown in Fig. 3.

Pomegranate peel contains groups such as alcohol, ester, ether and phenol groups. Functional groups in pomegranate peel deteriorate at high temperatures; therefore, a very simple CPP spectrum was obtained as seen in Fig. 3. The 2,322 cm⁻¹ band in the CPP spectrum is important such that it shows C≡C stretching peak of alkyne formed with thermal decomposition. The 2,104 cm⁻¹ band gives the O–H stretching peak of carboxylic acid found in the pomegranate peel. The absorption band at 1,990 cm⁻¹ is due to C=O stretching of lactones, ketones and carboxylic anhydrides [36,37]. The FTIR spectra of the adsorbent NZVI/CPP were investigated for before and after adsorption. The peaks at 2,341 and 2,353 cm⁻¹
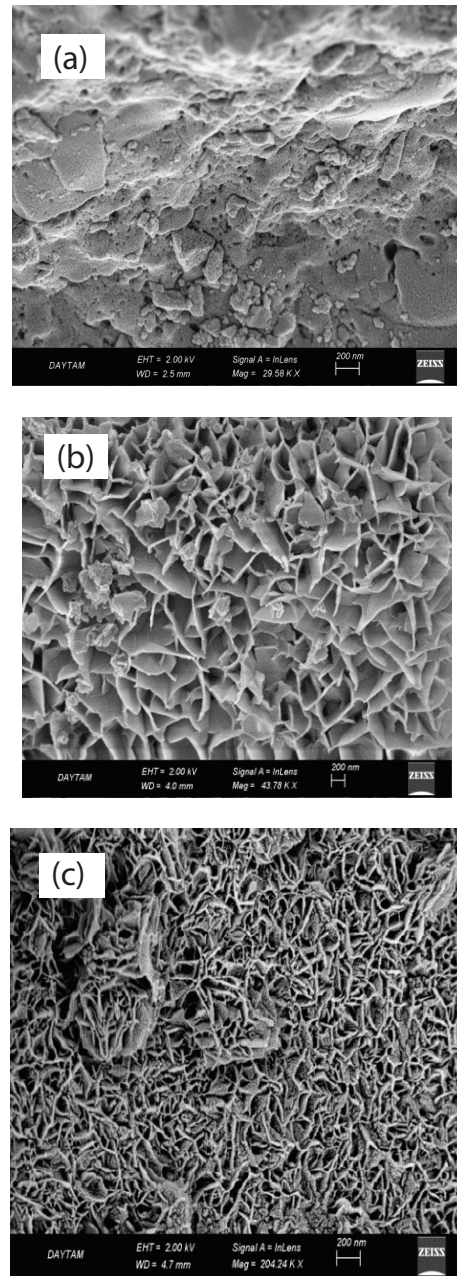
Fig. 2. SEM image of (a) CPP, (b) before and (c) after adsorption NZVI–CPP.
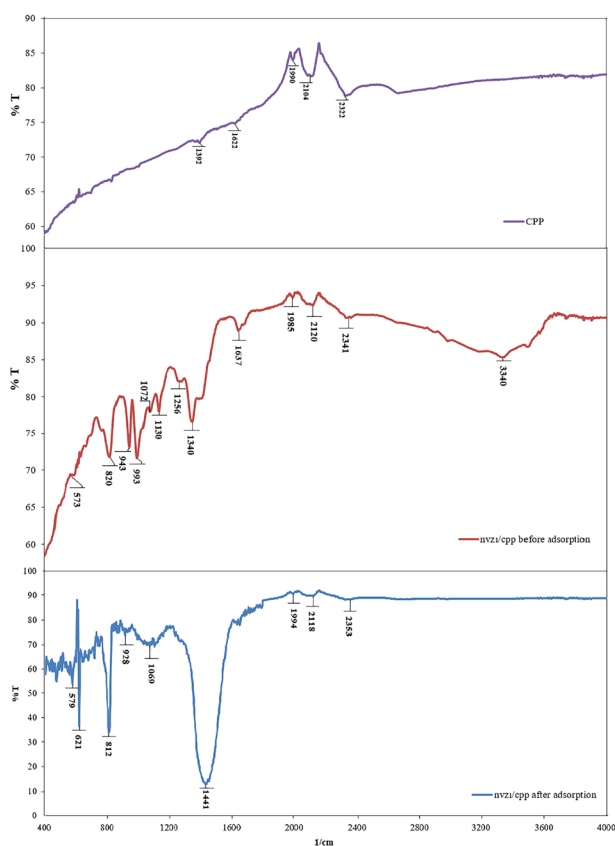
Fig. 3. FTIR spectrum of CPP, pre- and post-adsorption NZVI/CPP.

in Fig. 3 show C=C stretching of alkyne similar to CPP, the bands at 2,120 and 2,118 cm^{-1} represent O–H stretching of carboxylic acid, and the peaks at 1,985 and 1,994 cm^{-1} show C=O stretching of lactones, ketones and carboxylic anhydrides as in CPP [37]. The 1,637 and 1,622 cm^{-1} peaks represent CO stretching of the carboxylic acid in pomegranate peel and 1,392 cm^{-1} shows OCH, CCH and COH bending in CPP [38]. These peaks are due to the compounds found in the pomegranate peel structure. The NZVI/CPP adsorbent was prepared by applying some chemical treatments on CPP. Therefore, the spectrum of NZVI/CPP adsorbent was very complex. The characteristic absorption band at 3,340 cm^{-1} of NZVI/CPP is due to stretching vibration of O–H bond in ferric hydroxide on the surface after the reaction [35]. The peaks at 1,340 and 1,441 cm^{-1} indicate the ethanol used to prepare the NZVI/CPP [35]. It is thought that adsorption of MG increased the intensity of the 1,441 cm^{-1} peak [1]. The band at 1,256 cm^{-1} shows –COO bond within PEG. The peaks between 1,050 and 1,150 cm^{-1} show C–O–C bond within PEG [39]. The bands at 943 and 993 cm^{-1} give the bending bands for hydroxyl groups of ferric hydroxide. The 820 and 812 cm^{-1} peaks represent iron oxides formed by oxidation of Fe^0 [9,35]. Additionally, the adsorption bands at 573 and 579 cm^{-1} show stretching vibration of metal oxides [40,41]. These peaks prove the formation of the nanocomposite by NZVI loading on CPP.

The surface areas of the adsorbents were found using Quantachrome Corporation, Autosorb-6 model at 77 K. The samples were subjected to degassing in a cylindrical sample tube at 100°C under vacuum for 3 h before measurement. They were then analyzed under liquid nitrogen. The Brunauer–Emmett–Teller (BET) surface areas were calculated from the Brunauer Emmett Teller isotherm using the amount of nitrogen adsorbed at a relative pressure range (P/P_o) of 0.05–0.3. The surface areas of raw organic wastes are very low, so their surface areas are increased by pretreatments such as carbonization and activation. Angın et al. [42] increased the surface area of safflower seed press cake to 14.14 m^2/g by pyrolysis, activation with ZnCl$_2$ and carbonization processes. In another study, the surface area of the durian shell was increased to 8.41 m^2/g by pretreatment [43]. Gündüz and Bayrak [9] found the surface area of raw pomegranate peel as 1.83 m^2/g. The surface area was increased to 25.2 m^2/g by the processes applied on the adsorbent in their study. The CPP surface area was 2.23 m^2/g and the surface areas of pre- and post-adsorption cases were 25.2 and 23.49 m^2/g, respectively, for NZVI/CPP.

The X-ray diffraction (XRD) technique was applied at 2θ = 10°–100° and 1°/min scanning rate for the CPP and NZVI/CPP samples using a GNR explorer. The XRD patterns of the adsorbents were obtained at 40 kV/40 mA with a high-powered Cu-Kα radioactive source as shown in Fig. 4.

When the XRD patterns of CPP were examined, broad peaks appeared at 24.4° and 43.2° in 2θ (Fig. 4(a)). The peaks were obtained to be broad due to the amorphous structure of CPP. The XRD pattern showed that the adsorbent had a cellulosic, hemicellulosic and lignin structure. The XRD pattern of NZVI/CPP contained several peaks in Fig. 4(b). The peak at 45.06° belongs to zero valent iron (Fe^0). The peaks at 30°, 30.46°, 31.5°, 35° and 20.25° show the presence of γ-Fe$_2$O$_3$. The part of Fe° may be converted to γ-Fe$_2$O$_3$ in drying of NZVI/CPP. The peaks at 15.45°, 38.50°, 42.1° and 49.03° indicate the existence of γ-FeOOH. γ-FeOOH forms when zero-valent Fe is synthesized [35].

The pH$_{zpc}$ value is a parameter that should be known in order to understand the behavior of the adsorbent in different pH solutions. 0.01 M sodium chloride solution was prepared to determine the pH$_{zpc}$ value of the adsorbent NZVI/CPP, this solution was partitioned into six parts of 50 mL and each was adjusted to six different pH values in the range of 2–12. Then, 0.2 g of NZVI/CPP was added into each solution. The solutions were mixed for 10 min, left for equilibration at 20°C for 24 h. The pH values of the final solutions were measured. The difference (ΔpH) between the initial and final pH was plotted against the initial pH. The pH$_{zpc}$ value is the point where the curve of ΔpH vs. pH$_i$ crosses the line equal to zero [8,9]. The pH$_{zpc}$ value of NZVI/CPP was found to be 9.2.

3.2. Effect of initial MG concentration on adsorption

The effects of several MG concentrations ranging from 30 to 60 mg/L on adsorption were investigated and the results are given in Fig. 5(a). When the initial MG concentration was changed from 30 to 60 mg/L, % removal reduced from 98.46 to 93.04 and the q_e changed from 14.77 to 27.91 mg/g. % Removal decreased the higher initial dye concentration since the active sites reached saturation for the same amount of adsorbent at these concentrations [1,44,45]. In recent years, simultaneous adsorption and photocatalysis processes have been carried out to increase the efficiency of adsorption.
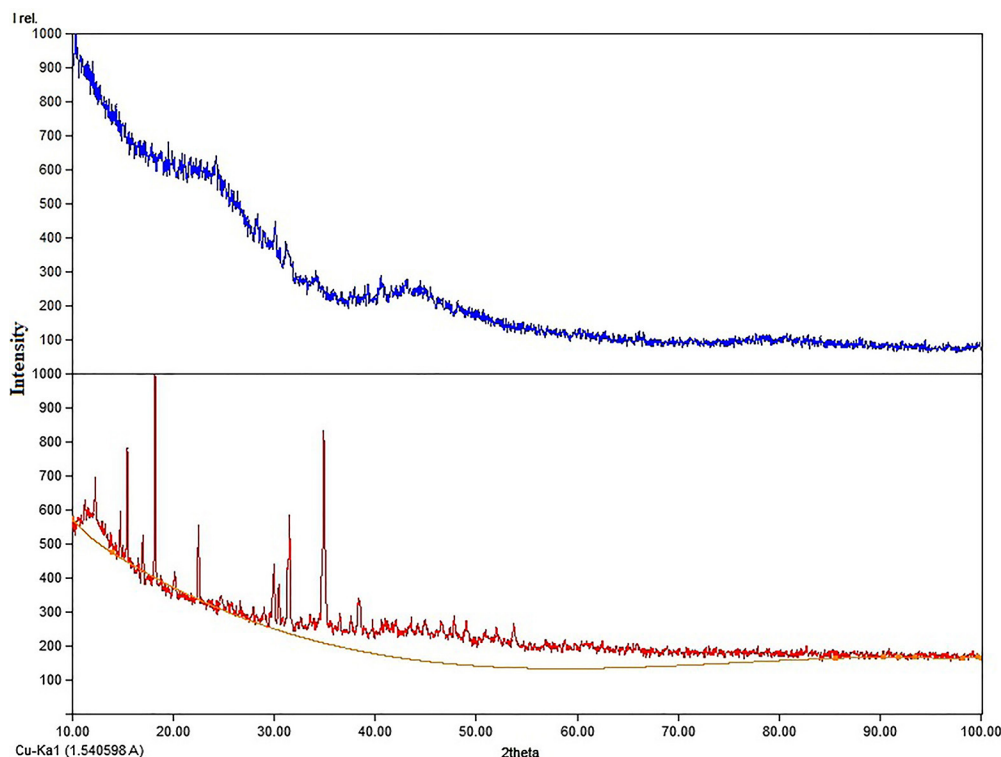
Fig. 4. XRD patterns of CPP (a) and NZVI/CPP (b).

When it was compared with these studies, it was found that attractiveness has been increased by waste pomegranate peel supported nanoiron and higher percentage removal values have been obtained [46,47].

3.3. Effect of initial solution pH

The effects of pH on adsorption are determined by two values which are the pK_a value and the pH_{zpc} (zero point charge) value of the adsorbent. The pK_a value of MG that was used in this study was 6.9 [9]. The pH_{zpc} value of the adsorbent NZVI/CPP was found as 9.2. If $pH > pK_a$, adsorbate (MG) is cationic, and if $pH < pK_a$, MG is anionic. This situation is different for the adsorbent. If $pH > pH_{zpc}$, the number of OH ions in the solution increases and the adsorbent surface is deprotonated. The adsorbent behaves like an anionic substance. On the contrary, the surface of NZVI/CPP is cationic for $pH < pH_{zpc}$ [9,37,48].

If pH is lower than 6.9, MG becomes anionic, and NZVI/CPP becomes cationic when pH is lower than 9.2. Thus, the MG becomes anionic and NZVI/CPP becomes cationic when pH < 6.9. For this reason, removal of MG increases till pH = 7 because of electrostatic attraction among the adsorbent and the adsorbate. If 6.9 < pH < 9.2, removal rate does not change up to pH 9.2, because MG becomes cationic and only the van der Waals forces are effective in this pH range.

When pH is greater than 9.2, the adsorbent turns anionic. Thus, electrostatic attraction increases again between the anionic adsorbent and cationic dye. The adsorption rate increases with the effect of ionic forces in addition to the van der Waals forces.

The effect of pH on adsorption of MG is given in Fig. 5(b). It was seen that the removal percentage of MG increased from 80.82% to 88.83% when the pH value was increased from 3 to 7 and it was almost fixed from 90.3% to 90.73% with a variation of pH from 8 to 9 and raised to 95.65% at pH = 10.

In a study by Dahri et al. [49], the change in color intensity of MG was investigated by changing the pH without adding an adsorbent. The color intensity did not change for pH values in range of 3.8–4.7 and they decreased by 10%–20% in the measurements made for pH 3.1, 6.2, 7.3 and 8.6. The color intensity decreased by up to 60% due to the formation of MGH^{+2} at pH < 2 and alkaline fading at pH > 10. pH values of lower than 2 and higher than 10 were not studied. Subramani and Thinakaran [50] examined the removal of several dyes with chitosan and found that removal of MG increased till pH = 7 and did not change too much after 7. In another study, removal of MG on CPP was studied at pH 4–9 and it was found that the percentage of removal increased with variation of pH from 4 to 6 and did not vary significantly by changing pH from 6 to 9 [9].

3.4. Effect of NZVI/CPP amount

The adsorbent dosage vs. removal of MG and adsorption capacity is shown in Fig. 5(c). The % removal increased from 86.65% to 99.69% and q_e varied from 172.13 to 13.29 mg/g when the adsorbent dosage was changed from 0.01 to 0.15 g. The increase in removal efficiency may be because of the increase in surface areas and active sites on NZVI/CPP. The decrease in q_e may depend on unsaturation of adsorption sites by reasons of overlapping and aggregation of excess amounts of NZVI/CPP [2,51].
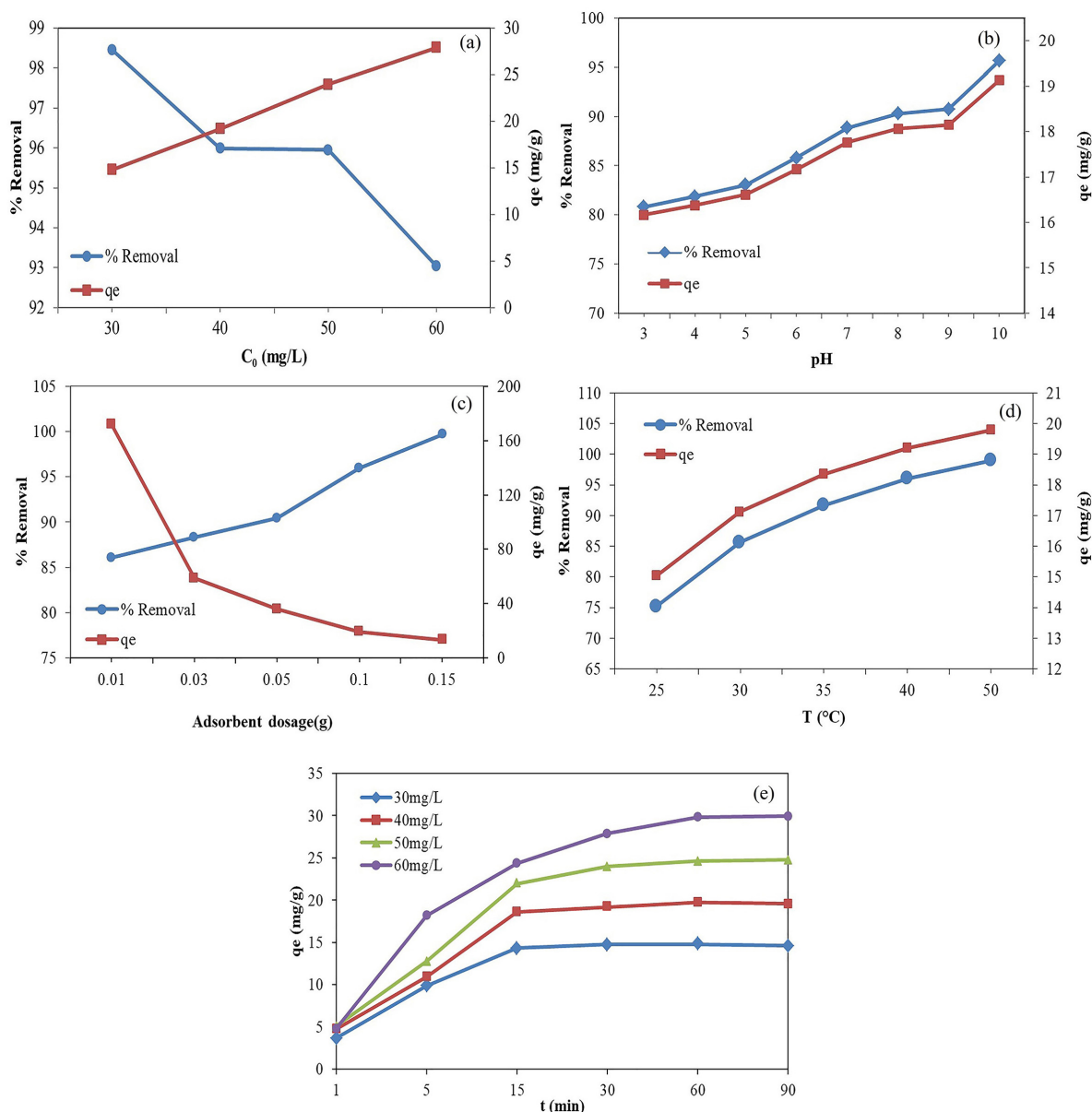
Fig. 5. The changes in % removal and q_e with examined parameters ((a)the effect of initial concentration, (b)the effect of pH, (c) the effect of adsorbent dosage, (d) the effect of temperature, (e) the effect of contact time) (T = 40°C, pH = 5.0 adsorbent amount = 0.1 g, C_0 = 40 mg/L and t = 30 min).

3.5. The change in adsorption capacity by contact time and initial MG concentration

Fig. 5(e) shows the effects of contact time and four different concentrations of MG on adsorption efficiency. It was observed that q_e increased by increasing the contact time up to 15 min in all solution concentrations. This was because there were abundantly active sites on the surface of NZVI/CPP, and mass transfer driving force caused by the initial MG concentration breaks the resistance between the adsorbent and adsorbate phases [44]. It slowed down between 15 and 30 min due to the saturation of active sites [1,44,45], and after 30 min, the change was negligible. The equilibrium q_e value changed from 14.77 to 27.91 mg/g with the initial concentration of MG solutions which varied from 30 to 60 mg/L.

3.6. Adsorption isotherms

Adsorption equilibrium isotherms explain the interactions between adsorbate molecules and adsorbents [51,52]. In this study, the Langmuir, Freundlich, Redlich–Peterson, Dubinin–Radushkevich and Temkin isotherms [2] were analyzed using adsorption parameters and these are presented in Tables 1 and 2.

Besides, this is described as a separation factor shown with R_L for Langmuir isotherm [52].

$$R_L = \frac{1}{1 + K_L \cdot Co} \qquad (3)$$

Table 1
Isotherm models

Isotherm	Equation	Model constants	References
Langmuir	$\dfrac{C_e}{q_e} = \dfrac{1}{q_m K_L} + \dfrac{C_e}{q_m}$	K_L is the Langmuir constant	[53]
Freundlich	$\ln q_e = \ln K_F + \dfrac{1}{n}\ln C_e$	K_F is the Freundlich constant n is heterogeneity factor	[54,55]
Temkin	$q_e = \dfrac{RT}{b}\ln K_T + \dfrac{RT}{b}\ln C_e$	K_T is the equilibrium binding constant b is the Temkin constant	[56]
Dubinin–Radushkevich	$\ln q_e = \ln q_m - K_{DR}\varepsilon^2$ $\varepsilon = RT\ln\left[1 + \dfrac{1}{C_e}\right]$	K_{DR} is isotherm constant ε is Polanyi potential	[57]
Redlich–Peterson	$\ln\left(\dfrac{K_R C_e}{q_e} - 1\right) = \beta_R \ln C_e + \ln\alpha_R$	K_R and α_R is constant β_R is exponent of R-P isotherm	[58]

Table 2
Isotherm parameters obtained from different isotherm models (adsorbent amount: 0.1 g, contact time: 30 min, pH: 5 and temperature: 40°C)

Models	Isotherm constants				
Langmuir	q_m (mg/g)	K_L (L/mg)	R^2	R_L	Errors
	32.47	1.31	0.977	0.0248 (30 mg/L) 0.0187 (40 mg/L) 0.0150 (50 mg/L) 0.0126 (60 mg/L)	$\chi^2 = 0.90$ RMSE = 2.71
Freundlich	K_F (mg/g)(L/mg)$^{1/n}$	n (g/L)	R^2		$\chi^2 = 1{,}603.4$ RMSE = 44.07
	1.34	0.34	0.946		
Temkin	B_T	K_T (L/mg)	R^2		$\chi^2 = 0.35$ RMSE = 1.93
	5.98	22.86	0.922		
Dubinin–Radushkevich	q_m (mg/g)	K_{DR} (mol^2/J^2)	R^2	E (kJ/mol)	$\chi^2 = 0.35$ RMSE = 0.98
	25.09	6.0×10^{-8}	0.801	2.89	
Redlich–Peterson	K_R (L/mg)	β_R	R^2	α_R (L/mg)	$\chi^2 = 13.64$ RMSE = 5
	42.55	0.76	0.989	13.07	

This shows that adsorption was linear for $R_L = 1$, irreversible for $R_L = 0$, feasible for $0 < R_L < 1$ and unfeasible for $R_L > 1$ [1,2].

The B_T factor used in the Temkin isotherm was equal to RT/b. If the constant B_T has positive value, this indicates that the process is endothermic [59].

The mean adsorption energy (E) mentioned in the Dubinin–Radushkevich isotherm was used for estimation of the adsorption mechanism.

$$E = \frac{1}{\sqrt{2K_{DR}}} \qquad (4)$$

If $8 < E < 16$ kJ/mol, adsorption can be explained by ion exchange. When $E < 8$ kJ/mol, it is evaluated as physical adsorption. If it ranges from 20 to 40 kJ/mol, the process is considered to be chemical adsorption [52].

The Redlich–Peterson isotherm is an isotherm that includes the characteristics of both the Langmuir and Freundlich isotherms. As the β_R factor in the equation of Redlich–Peterson (R-P) model approaches 1, the process behaves like the Langmuir isotherm, and as β_R gets closer to zero, adsorption shows the behavior of the Freundlich isotherm [3,58].

The adsorption isotherms were used at 30, 40, 50 and 60 mg/L based on the experimental conditions described in Table 2. The isotherm constants and correlation coefficients (R^2) of the isotherm models are given in Table 2 and Fig. 6.

When the R^2 values were examined, the Langmuir and Redlich–Peterson isotherms were the best fits with the experimental data. In such a case, chi-square test (χ^2) and residual root-mean-square error (RMSE) are effective for deciding on one of the two models. χ^2 and RMSE values were calculated by the following equations:

$$\chi^2 = \sum_{i-1}^{n} \left[\frac{\left(Y_{exp} - Y_{cal}\right)^2}{Y_{cal}} \right] \tag{5}$$

$$RMSE = \sqrt{\frac{1}{n-p} \sum_{i-1}^{n} \left[\left(Y_{exp} - Y_{cal}\right)^2 \right]} \tag{6}$$

where Y_{exp} is the experimental data, Y_{cal} is the calculated data from the model and n is the number of experimental data. The lowest values of χ^2 and RMSE ensure us to make the right decision between the two models [60]. The lowest χ^2 and RMSE values were obtained in the Langmuir isotherm. Therefore, the Langmuir model with $R^2 = 0.977$ value fit better than other models for the adsorption process of MG on NZVI/CPP [7,51].

The n value was 0.34 g/L in the Freundlich isotherm, which means that adsorption was a physical process when $n < 1$. For the Temkin isotherm, since B_T was 5.98 kJ/mol, the adsorption was endothermic. The E value in the D-R isotherm was 2.89 kJ/mol. Therefore, the process was physical adsorption and it approached the Langmuir isotherm as the β value was 0.76 for the R-P isotherm.

3.7. Adsorption kinetics

Adsorption kinetics were analyzed using integrated equations and the experimental data for pseudo-first-order/pseudo-second-order, intraparticle diffusion and the Elovich model (Tables 3 and 4) [61–64].

When the R^2 values in Table 4 and Fig. 7 were examined for all kinetic models, the pseudo-second-order model was the most suitable kinetic model for this process, because it had the highest R^2 values. Besides, when the experimentally found q_e values were compared with the obtained q_e values, it was found that these two sets of values were very close to each other.

3.8. Effects of temperature on MG adsorption and thermodynamic parameters

% Removal of dye and adsorption capacity were examined for temperatures in the range of 25°C–50°C and it was shown that these factors increased with the rise in temperature, therefore, the adsorption was endothermic. While the removal of dye was 75.23% at 25°C, and it reached 98.94% at 50°C. The q_e of adsorbent increased from 15.05 mg/g at 25°C to 19.79 mg/g at 50°C (Fig. 5(d)). The reason for this increase by temperature was the expansion of pores and formation of new active sites due to bond cleavage on the NZVI/CPP surface. Furthermore, the diffusion rate of the MG molecules into the pores on the NZVI/CPP surface also increased with the rise in temperature [4,6,8,52].

Thermodynamics parameters were standard free energy $\Delta G°$ (kJ/mol), entropy $\Delta S°$ (kJ/mol K) and enthalpy $\Delta H°$ (kJ/mol), and these were obtained by utilizing the following equations.

$$K_D = \frac{q_e}{C_e} \tag{7}$$

where K_D is the distribution coefficient representing the affinity of the NZVI/CPP surface.

$\Delta G°$ was calculated as follows:

$$\Delta G^o = -RT \ln K_D \tag{8}$$

where $R = 8.314$ J/mol K and T (K) is the temperature.

When $\ln K_D$ was plotted against $1/T$, the values of $\Delta S°$ and $\Delta H°$ were found using the intercept and slope from the Van't Hoff equation given below, respectively [6,44].

$$\ln K_D = \frac{\Delta S°}{R} - \frac{\Delta H°}{RT} \tag{9}$$

Another piece of evidence that the adsorption was endothermic is $\Delta H° > 0$ as seen in Table 5. The value of $\Delta G°$ was negative and it decreased when the temperature was increased. So, the adsorption took place spontaneously and spontaneity increased as the temperature increased. The positive $\Delta S°$ shows that the degrees of disorder increased slightly in the adsorbent–adsorbate interface. It was reported in the literature that the process was physisorption for $\Delta G° > -20$ kJ/mol, chemisorption between -80 and -400 kJ/mol [6,65]. The values of $\Delta G°$ ranged from -0.89 to -10.21 kJ/mol. Therefore, the adsorption was physisorption.

3.9. Comparison with various adsorbents of NZVI/CPP

Table 6 shows the maximum adsorption capacities of different adsorbents for the adsorption of MG from aqueous solutions. Although several materials have been used as adsorbents to remove MG, adsorbents supported by NZVI have not been used. When the adsorbents were examined in terms of their maximum adsorption capacity, the equilibration time and the amount of adsorbent used, NZVI/CPP was found to be a considerable adsorbent.

4. Conclusion

NZVI supported by CPP was produced as a new composite material by liquid-phase chemical reduction in this study and used as an adsorbent to dispose of MG. The surface characteristics of NZVI/CPP were determined by FTIR, SEM, XRD and BET analyses. Isotherms commonly used in aqueous solutions were applied on the experimental data and it was found that the most suitable model was the Langmuir isotherm. A kinetic model was

Table 3
Kinetic models applied for adsorption

Kinetic model	Integrated equation	Model constants	References
Pseudo-first-order	$\log\left(q_e - q_t\right) = \log q_e - \dfrac{K_1}{2.303}t$	K_1 is pseudo-first-order rate constant	[7,62]
Pseudo-second-order	$\dfrac{1}{q_t} = \dfrac{1}{K_2 q_e^2} + \dfrac{t}{q_e}$	K_2 is second-order rate constant	[61]
Elovich	$q_t = \dfrac{1}{\beta}\ln\left(\alpha.\beta\right) + \dfrac{1}{\beta}\ln\left(t\right)$	α and β are Elovich constants	[63]
Intraparticle diffusion	$q_t = K_i t^{1/2} + C$	K_i is intraparticle diffusion constant	[64]

Table 4
Kinetic constants for different kinetic model

Models	Kinetic constants			
Pseudo-first-order model	K_1 (1/min)	q_e (mg/g)	R^2	q_e (mg/g) (experimental)
30 mg/L	85×10^{-3}	6.42	0.543	14.77
40 mg/L	98×10^{-3}	9.93	0.638	19.20
50 mg/L	103×10^{-3}	16.93	0.921	23.99
60 mg/L	103×10^{-3}	19.79	0.973	27.91
Pseudo-second-order model	K_2 (mg/g min)	q_e (mg/g)	R^2	q_e (mg/g) (experimental)
30 mg/L	19×10^{-3}	16.53	0.998	14.77
40 mg/L	12×10^{-3}	21.98	0.994	19.20
50 mg/L	7×10^{-3}	28.17	0.996	23.99
60 mg/L	6×10^{-3}	32.57	0.997	27.91
Elovich model	α (mg/g min)	β (mg/g min)	R^2	
30 mg/L	11.19	0.29	0.973	
40 mg/L	12.54	0.22	0.967	
50 mg/L	13.02	0.18	0.981	
60 mg/L	15.70	0.15	0.987	
Intraparticle diffusion model	K_i (mg/g min$^{1/2}$)	C	R^2	
30 mg/L	2.45	2.96	0.858	
40 mg/L	3.34	2.89	0.899	
50 mg/L	4.32	2.38	0.932	
60 mg/L	4.90	3.40	0.884	

Table 5
Thermodynamic parameters

T (°C)	$\Delta H°$ (kJ/mol)	$\Delta S°$ (kJ/mol K)	$\Delta G°$ (kJ/mol)
25	110.27	0.37	−0.89
30			−2.75
35			−4.62
40			−6.48
50			−10.21

determined as a pseudo-second-order model by means of experimental studies carried out to determine the mechanisms controlling the rate of adsorption. When the thermodynamics of adsorption was examined, it was found that the process occurred endothermically ($\Delta H° > 0$) and spontaneously ($\Delta G° < 0$). The degrees of disorder increased in the adsorption process for $\Delta S° > 0$. Pomegranate peel used as a supportive element for NZVI is a waste material; hence, it has low cost and it is effective as an adsorbent in the removal of MG.

Table 6
The comparison of various adsorbents of NZVI/CPP for adsorption of MG

Adsorbents	q_m (mg/g)	Equilibrium time	pH	Adsorbent dose	References
Polyaniline–nickel ferrite magnetic nanocomposite	4.09	210 min	7	5 g/L	[66]
Peat	143.68	4 h	Ambient	0.1 g/50 mL	[67]
Breadfruit skin	55.2 mg/g	3.5 h	4.58	–	[68]
Graphene oxide/cellulose bead composites	30.09	12 h	7	0.1 g	[69]
Cadmium hydroxide nanowires loaded on activated carbon	19	30–50 min	5	0.02–0.03 g	[70]
Arundo donax root carbon	9.35	180 min	5	0.6 g/100 mL	[71]
Peroxide treated rice husk	26.6	90 min	8	200 mg/100 mL	[72]
Perlite	3.36	40 min	8–9	0.1 g/50 mL	[73]
Sulfuric acid treated *Parthenium hysterophorus* Linn.	16.81	90 min	7	0.2 g/50 mL	[74]
NZVI/CPP	32.47	30 min	5	0.1 g/50 mL	In this study
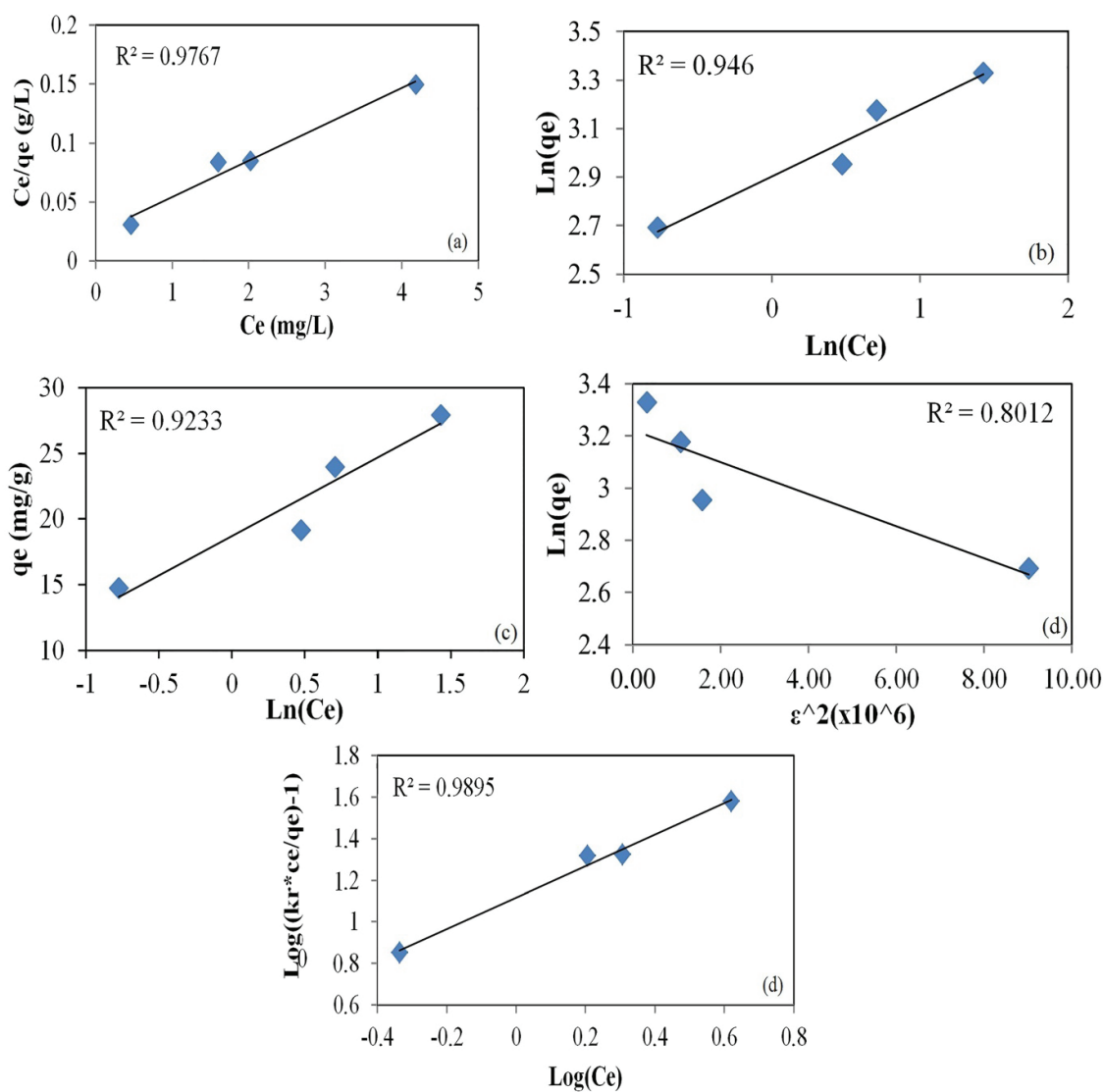
Fig. 6. Isotherm curves for (a) Langmuir, (b) Freundlich, (c) Temkin, (d) Dubinin–Radushkevich and (e) Redlich–Peterson (adsorbent amount: 0.1 g; contact time: 30 min, pH: 5 and temperature: 40°C).
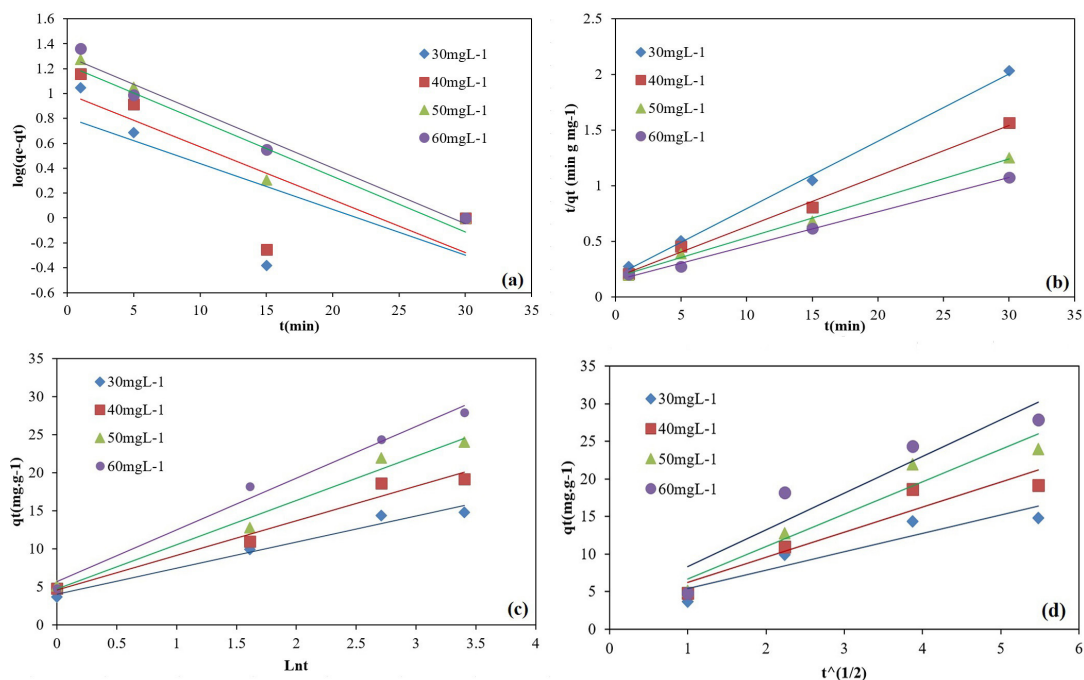
Fig. 7. Linearized plots of (a) a pseudo-first-order, (b) a pseudo-second-order, (c) the Elovich model and (d) the intraparticle diffusion model in different concentrations at 40°C.

References

[1] S. Banerjee, G.C. Sharma, R.K. Gautam, M.C. Chattopadhyaya, S.N. Upadhyay, Y.C. Sharma, Removal of Malachite Green, a hazardous dye from aqueous solutions using *Avena sativa* (oat) hull as a potential adsorbent, J. Mol. Liq., 213 (2016) 162–172.

[2] M.R.R. Kooh, M.K. Dahri, L.B.L. Lim, L.H. Lim, O.A. Malik, Batch adsorption studies of the removal of methyl violet 2B by soya bean waste: isotherm, kinetics and artificial neural network modelling, Environ. Earth Sci., 75 (2016) 1–14.

[3] H. Shayesteh, A. Rahbar-Kelishami, R. Norouzbeigi, Adsorption of malachite green and crystal violet cationic dyes from aqueous solution using pumice stone as a low-cost adsorbent: kinetic, equilibrium, and thermodynamic studies, Desal. Wat. Treat., 57 (2016) 12822–12831.

[4] Y.H. Song, S.G. Ding, S.M. Chen, H. Xu, Y. Mei, J.M. Ren, Removal of malachite green in aqueous solution by adsorption on sawdust, Korean J. Chem. Eng., 32 (2015) 2443–2448.

[5] M.A. Ahmad, R. Alrozi, Optimization of preparation conditions for mangosteen peel-based activated carbons for the removal of Remazol Brilliant Blue R using response surface methodology, Chem. Eng. J., 165 (2010) 883–890.

[6] A. Reffas, A. Bouguettoucha, D. Chebli, A. Amrane, Adsorption of ethyl violet dye in aqueous solution by forest wastes, wild carob, Desal. Wat. Treat., 57 (2016) 9859–9870.

[7] G. Karaçetin, S. Sivrikaya, M. Imamoğlu, Adsorption of methylene blue from aqueous solutions by activated carbon prepared from hazelnut husk using zinc chloride, J. Anal. Appl. Pyrolysis, 110 (2014) 270–276.

[8] K. Saeed, M. Ishaq, S. Sultan, I. Ahmad, Removal of methyl violet 2-B from aqueous solutions using untreated and magnetite-impregnated almond shell as adsorbents, Desal. Wat. Treat., 57 (2016) 13484–13493.

[9] F. Gündüz, B. Bayrak, Biosorption of malachite green from an aqueous solution using pomegranate peel: equilibrium modelling, kinetic and thermodynamic studies, J. Mol. Liq., 243 (2017) 790–798.

[10] M.K. Uddin, A review on the adsorption of heavy metals by clay minerals, with special focus on the past decade, Chem. Eng. J., 308 (2017) 438–462.

[11] Z. Ma, Q. Zhang, X. Weng, C. Mang, L. Si, Z. Guan, L. Cheng, Fluoride ion adsorption from wastewater using magnesium(II), aluminum(III) and titanium(IV) modified natural zeolite: kinetics, thermodynamics, and mechanistic aspects of adsorption, J Water Reuse Desal., 8 (2017). doi: 10.2166/wrd.2017.037.

[12] O. Lacin, B. Bayrak, O. Korkut, E. Sayan, Modeling of adsorption and ultrasonic desorption of cadmium(II) and zinc(II) on local bentonite, J. Colloid Interface Sci., 292 (2005) 330–335.

[13] O. Korkut, E. Sayan, O. Lacin, B. Bayrak, Investigation of adsorption and ultrasound assisted desorption of lead (II) and copper (II) on local bentonite: a modelling study, Desalination, 259 (2010) 243–248.

[14] N.K. Amin, Removal of direct blue-106 dye from aqueous solution using new activated carbons developed from pomegranate peel: adsorption equilibrium and kinetics, J. Hazard. Mater., 165 (2009) 52–62.

[15] A. Bhatnagar, A.K. Minocha, Adsorptive removal of 2,4-dichlorophenol from water utilizing *Punica granatum* peel waste and stabilization with cement, J. Hazard. Mater., 168 (2009) 1111–1117.

[16] Ç.Ö. Ay, A.S. Özcan, Y. Erdoğan, A. Özcan, Characterization of *Punica granatum* L. peels and quantitatively determination of its biosorption behavior towards lead (II) ions and Acid Blue 40, Colloids Surf., B, 100 (2012) 197–204.

[17] T. Senthilkumar, R. Raghuraman, L.R. Miranda, Parameter optimization of activated carbon production from *Agave sisalana* and *Punica granatum* peel: adsorbents for CI reactive orange 4 removal from aqueous solution, Clean Soil Air Water, 41 (2013) 797–807.

[18] T.S. Najim, S.A. Yassin, Removal of chromium from aqueous solution using modified pomegranate peel: mechanistic and thermodynamic studies, J. Chem., 6 (2009) S153–S158.

[19] G. Sharma, D. Kumar, A. Kumar, H. Ala'a, D. Pathania, M. Naushad, G.T. Mola, Revolution from monometallic to trimetallic nanoparticle composites, various synthesis methods and their applications: a review, Mater. Sci. Eng., C, 71 (2017) 1216–1230.

[20] R. Katwal, H. Kaur, G. Sharma, M. Naushad, D. Pathania, Electrochemical synthesized copper oxide nanoparticles for enhanced photocatalytic and antimicrobial activity, J. Ind. Eng. Chem., 31 (2015) 173–184.

[21] M. Khosravi, S. Arabi, Application of response surface methodology (RSM) for the removal of methylene blue dye from water by nano zero-valent iron (NZVI), Water Sci. Technol., 74 (2016) 343–352.

[22] P. Dorjee, D. Amarasiriwardena, B. Xing, Antimony adsorption by zero-valent iron nanoparticles (nZVI): ion chromatography–inductively coupled plasma mass spectrometry (IC–ICP-MS) study, Microchem. J., 116 (2014) 15–23.

[23] A.M. Azzam, S.T. El-Wakeel, B.B. Mostafa, M. El-Shahat, Removal of Pb, Cd, Cu and Ni from aqueous solution using nano scale zero valent iron particles, J. Environ. Chem. Eng., 4 (2016) 2196–2206.

[24] N. Ezzatahmadi, G.A. Ayoko, G.J. Millar, R. Speight, C. Yan, J. Li, S. Li, J. Zhu, Y. Xi, Clay-supported nanoscale zero-valent iron composite materials for the remediation of contaminated aqueous solutions: a review, Chem. Eng. J., 312 (2016) 336–350.

[25] Y. Xie, Y. Yi, Y. Qin, L. Wang, G. Liu, Y. Wu, Z. Diao, T. Zhou, M. Xu, Perchlorate degradation in aqueous solution using chitosan-stabilized zero-valent iron nanoparticles, Sep. Purif. Technol., 171 (2016) 164–173.

[26] N. Arancibia-Miranda, S.E. Baltazar, A. García, D. Munoz-Lira, P. Sepúlveda, M.A. Rubio, D. Altbir, Nanoscale zero valent supported by zeolite and montmorillonite: template effect of the removal of lead ion from an aqueous solution, J. Hazard. Mater., 301 (2016) 371–380.

[27] A. Afizah, A. Salina, D. Farrah Aini, S. Ragunathan, T.T. Tjoon, Kinetic removal of Cr^{6+} in aqueous solution by carboxymethyl cellulose-stabilized nano zero-valent iron particles, Maced. J. Chem. Chem. Eng., 34 (2015) 295–308.

[28] V. Alipour, S. Nasseri, R.N. Nodehi, A.H. Mahvi, A. Rashidi, Preparation and application of oyster shell supported zero valent nano scale iron for removal of natural organic matter from aqueous solutions, J. Environ. Health Sci. Eng., 12 (2014) 146.

[29] D. Prabu, R. Parthiban, P. Senthil Kumar, N. Kumari, P. Saikia, Adsorption of copper ions onto nano-scale zero-valent iron impregnated cashew nut shell, Desal. Wat. Treat., 57 (2016) 6487–6502.

[30] H. Zhu, Y. Jia, X. Wu, H. Wang, Removal of arsenic from water by supported nano zero-valent iron on activated carbon, J. Hazard. Mater., 172 (2009) 1591–1596.

[31] A. Kumar, C. Guo, G. Sharma, D. Pathania, M. Naushad, S. Kalia, P. Dhiman, Magnetically recoverable ZrO_2/Fe_3O_4/chitosan nanomaterials for enhanced sunlight driven photoreduction of carcinogenic Cr(VI) and dechlorination and mineralization of 4-chlorophenol from simulated waste water, RSC Adv., 6 (2016) 13251–13263.

[32] A.A. Alqadami, M. Naushad, M.A. Abdalla, M.R. Khan, Z.A. Alothman, Adsorptive removal of toxic dye using Fe_3O_4–TSC nanocomposite: equilibrium, kinetic, and thermodynamic studies, J. Chem. Eng. Data, 61 (2016) 3806–3813.

[33] G. Sharma, A. Kumar, M. Naushad, D. Pathania, M. Sillanpää, Polyacrylamide@Zr(IV) vanadophosphate nanocomposite: ion exchange properties, antibacterial activity, and photocatalytic behavior, J. Ind. Eng. Chem., 33 (2016) 201–208.

[34] G. Sharma, D. Pathania, M. Naushad, N. Kothiyal, Fabrication, characterization and antimicrobial activity of polyaniline Th(IV) tungstomolybdophosphate nanocomposite material: efficient removal of toxic metal ions from water, Chem. Eng. J., 251 (2014) 413–421.

[35] F. Yang, Y. He, S. Sun, Y. Chang, F. Zha, Z. Lei, Walnut shell supported nanoscale Fe^0 for the removal of Cu(II) and Ni(II) ions from water, J. Appl. Polym. Sci., 133 (2016) 43304–43309.

[36] S. Ben-Ali, I. Jaouali, S. Souissi-Najar, A. Ouederni, Characterization and adsorption capacity of raw pomegranate peel biosorbent for copper removal, J. Cleaner Prod., 142 (2017) 3809–3821.

[37] H. Singh, G. Chauhan, A.K. Jain, S. Sharma, Adsorptive potential of agricultural wastes for removal of dyes from aqueous solutions, J. Environ. Chem. Eng., 5 (2017) 122–135.

[38] M.B. Silveira, F.A. Pavan, N.F. Gelos, E.C. Lima, S.L. Dias, *Punica granatum* shell preparation, characterization, and use for crystal violet removal from aqueous solution, Clean Soil Air Water, 42 (2014) 939–946.

[39] B. Suart, Infrared Spectroscopy: Fundamental and Applications, John Wiley & Sons, Ltd., Canada, 2004.

[40] T. Tatarchuk, M. Bououdina, N. Paliychuk, I. Yaremiy, V. Moklyak, Structural characterization and antistructure modeling of cobalt-substituted zinc ferrites, J. Alloys Compd., 694 (2017) 777–791.

[41] T. Tatarchuk, N. Paliychuk, M. Bououdina, B. Al-Najar, M. Pacia, W. Macyk, A. Shyichuk, Effect of cobalt substitution on structural, elastic, magnetic and optical properties of zinc ferrite nanoparticles, J. Alloys Compd., 731 (2018) 1256–1266.

[42] D. Angın, E. Altintig, T.E. Köse, Influence of process parameters on the surface and chemical properties of activated carbon obtained from biochar by chemical activation, Bioresour. Technol., 148 (2013) 542–549.

[43] K. Foo, B. Hameed, Textural porosity, surface chemistry and adsorptive properties of durian shell derived activated carbon prepared by microwave assisted NaOH activation, Chem. Eng. J., 187 (2012) 53–62.

[44] M.A. Ahmad, R. Alrozi, Removal of malachite green dye from aqueous solution using rambutan peel-based activated carbon: equilibrium, kinetic and thermodynamic studies, Chem. Eng. J., 171 (2011) 510–516.

[45] E.-K. Guechi, O. Hamdaoui, Biosorption of methylene blue from aqueous solution by potato (*Solanum tuberosum*) peel: equilibrium modelling, kinetic, and thermodynamic studies, Desal. Wat. Treat., 57 (2016) 10270–10285.

[46] D. Pathania, R. Katwal, G. Sharma, M. Naushad, M.R. Khan, H. Ala'a, Novel guar gum/Al_2O_3 nanocomposite as an effective photocatalyst for the degradation of malachite green dye, Int. J. Biol. Macromol., 87 (2016) 366–374.

[47] G. Sharma, M. Naushad, D. Pathania, A. Kumar, A multifunctional nanocomposite pectin thorium (IV) tungstomolybdate for heavy metal separation and photoremediation of malachite green, Desal. Wat. Treat., 57 (2016) 19443–19455.

[48] R.A. Rao, F. Rehman, Adsorption of heavy metal ions on pomegranate (*Punica granatum*) peel: removal and recovery of Cr(VI) ions from a multi-metal ion system, Adsorpt. Sci. Technol., 28 (2010) 195–211.

[49] M.K. Dahri, M.R.R. Kooh, L.B.L. Lim, Water remediation using low cost adsorbent walnut shell for removal of malachite green: equilibrium, kinetics, thermodynamic and regeneration studies, J. Environ. Chem. Eng., 2 (2014) 1434–1444.

[50] S. Subramani, N. Thinakaran, Isotherm, kinetic and thermodynamic studies on the adsorption behaviour of textile dyes onto chitosan, Process Saf. Environ. Prot., 106 (2017) 1–10.

[51] L.-G. Wang, G.-B. Yan, Adsorptive removal of direct yellow 161dye from aqueous solution using bamboo charcoals activated with different chemicals, Desalination, 274 (2011) 81–90.

[52] M. Ghasemi, S. Mashhadi, M. Asif, I. Tyagi, S. Agarwal, V.K. Gupta, Microwave-assisted synthesis of tetraethylenepentamine functionalized activated carbon with high adsorption capacity for Malachite green dye, J. Mol. Liq., 213 (2016) 317–325.

[53] I. Langmuir, The adsorption of gases on plane surfaces of glass, mica and platinum, J. Am. Chem. Soc., 40 (1918) 1361–1403.

[54] H. Freundlich, Uber die adsorption in lasugen (Leipzig), Z. Phys. Chem. A, 57 (1906) 385–470.

[55] L. Zhang, H. Zhang, W. Guo, Y. Tian, Removal of malachite green and crystal violet cationic dyes from aqueous solution using activated sintering process red mud, Appl. Clay Sci., 93 (2014) 85–93.

[56] M. Temkin, V. Pyzhev, Recent Modifications to Langmuir Isotherms, Acta Physiochim, 12 (1940) 217–222.

[57] M. Dubinin, L. Radushkevich, Equation of the characteristic curve of activated charcoal, Chem. Zentr, 1 (1947) 875–890.

[58] O. Redlich, D.L. Peterson, A useful adsorption isotherm, J. Phys. Chem., 63 (1959) 1024.

[59] M.A. Ahmad, N. Ahmad, O.S. Bello, Modified durian seed as adsorbent for the removal of methyl red dye from aqueous solutions, Appl. Water Sci., 5 (2015) 407–423.

[60] M. Baghdadi, B.A. Soltani, M. Nourani, Malachite green removal from aqueous solutions using fibrous cellulose sulfate prepared from medical cotton waste: comprehensive batch and column studies, J. Ind. Eng. Chem., 55 (2017) 128–139.

[61] Y.-S. Ho, G. McKay, Pseudo-second order model for sorption processes, Process Biochem., 34 (1999) 451–465.

[62] S. Lagergren, Zur theorie der sogenannten adsorption geloster stoffe, K. Sven. Vetensk.akad. Handl., 24 (1898) 1–39.

[63] M. Low, Kinetics of chemisorption of gases on solids, Chem. Rev., 60 (1960) 267–312.

[64] W.J. Weber, J.C. Morris, Kinetics of adsorption on carbon from solution, J. Sanit. Eng. Div., 89 (1963) 31–60.

[65] T. Şahan, D. Öztürk, Investigation of Pb(II) adsorption onto pumice samples: application of optimization method based on fractional factorial design and response surface methodology, Clean Technol. Environ. Policy, 16 (2014) 819–831.

[66] M.R. Patil, V. Shrivastava, Adsorption of malachite green by polyaniline–nickel ferrite magnetic nanocomposite: an isotherm and kinetic study, Appl. Nanosci., 5 (2015) 809–816.

[67] H.I. Chieng, T. Zehra, L.B.L. Lim, N. Priyantha, D. Tennakoon, Sorption characteristics of peat of Brunei Darussalam IV: equilibrium, thermodynamics and kinetics of adsorption of methylene blue and malachite green dyes from aqueous solution, Environ. Earth Sci., 72 (2014) 2263–2277.

[68] L.B.L. Lim, N. Priyantha, N.H. Mohd Mansor, Utilizing *Artocarpus altilis* (breadfruit) skin for the removal of malachite green: isotherm, kinetics, regeneration, and column studies, Desal. Wat. Treat., 57 (2016) 16601–16610.

[69] X. Zhang, H. Yu, H. Yang, Y. Wan, H. Hu, Z. Zhai, J. Qin, Graphene oxide caged in cellulose microbeads for removal of malachite green dye from aqueous solution, J. Colloid Interface Sci., 437 (2015) 277–282.

[70] M. Ghaedi, N. Mosallanejad, Study of competitive adsorption of malachite green and sunset yellow dyes on cadmium hydroxide nanowires loaded on activated carbon, J. Ind. Eng. Chem., 20 (2014) 1085–1096.

[71] J. Zhang, Y. Li, C. Zhang, Y. Jing, Adsorption of malachite green from aqueous solution onto carbon prepared from Arundo donax root, J. Hazard. Mater., 150 (2008) 774–782.

[72] B. Ramaraju, P. Manoj Kumar Reddy, C. Subrahmanyam, Low cost adsorbents from agricultural waste for removal of dyes, Environ. Prog. Sustain. Energy, 33 (2014) 38–46.

[73] V. Govindasamy, R. Sahadevan, S. Subramanian, D.K. Mahendradas, Removal of malachite green from aqueous solutions by perlite, Int. J. Chem. Reactor Eng., 7 (2009) 43–49.

[74] H. Lata, R.K. Gupta, V.K. Garg, Removal of basic dye from aqueous solution using chemically modified *Parthenium hysterophorus* Linn. biomass, Chem. Eng. Commun., 195 (2008) 1185–1199.